Frequency Comb Generation in Superconducting Resonators

R. P. Erickson, M. R. Vissers, M. Sandberg, S. R. Jefferts, and D. P. Pappas*
National Institute of Standards and Technology, Boulder, Colorado 80305, USA
(Received 20 June 2014; revised manuscript received 27 August 2014; published 30 October 2014)

We have generated frequency combs spanning 0.5 to 20 GHz in superconducting $\lambda/2$ resonators at $T = 3$ K. Thin films of niobium-titanium nitride enabled this development due to their low loss, high nonlinearity, low frequency dispersion, and high critical temperature. The combs nucleate as sidebands around multiples of the pump frequency. Selection rules for the allowed frequency emission are calculated using perturbation theory, and the measured spectrum is shown to agree with the theory. Sideband spacing is measured to be accurate to 1 part in 10^8. The sidebands coalesce into a continuous comb structure observed to cover at least several frequency octaves.

DOI: 10.1103/PhysRevLett.113.187002 PACS numbers: 85.25.Pb, 03.67.Lx, 07.57.Kp, 85.25.Oj

Frequency combs in the optical regime have become extremely useful in a wide range of applications including spectroscopy and frequency metrology [1–3]. Recently, it was found that a strongly pumped, high-Q optical microcavity made from a nonlinear medium generates sidebands due to a combination of degenerate and nondegenerate four-wave mixing (FWM) [4–6] that cascade into a broadband frequency comb of photon energies in the regime of hundreds of THz. The peaks of these combs are extremely narrow and appear at frequencies dictated by selection rules for photon energy and momentum conservation. These devices are attractive because they have very narrow linewidths, are relatively simple, highly stable and controllable [7–9], and can be divided down into the GHz range to achieve very accurate frequency references. For these microcavities, typically consisting of toroidal silica structures [10], comb generation over much more than a single octave in frequency is difficult to obtain due to frequency dispersion from material and geometric factors, which make the modes nonequidistant.

These Kerr combs continue to be the focus of extensive theoretical analysis to understand the nonlinear dynamics that give rise to their threshold of stability, mechanism of cascade, amplitude of responsiveness, and maximum spectral bandwidth [11–15]. Generation of these combs directly in the 1–20 GHz range would further simplify the instrumentation and potentially elucidate the dynamics involved by making them more accessible to direct measurement.

In the current Letter, we transfer the nonlinear pumped cavity concept to the microwave regime in superconducting resonators and demonstrate broadband frequency comb generation over multiple octaves. This is achieved using niobium-titanium nitride (NbTiN) thin films and exploiting (i) the high quality factor $Q > 10^7$ for a strong drive [16,17], (ii) the large nonlinear kinetic inductance, and (iii) the lack of frequency dispersion [18]. The kinetic inductance, $L_r(t) = L_0\{1 + [I(t)/I_*]^2\}$, where L_0 is the geometric inductance and I_* a normalization constant comparable to the critical current, arises from the stored kinetic energy of charge carriers.

The nonlinear kinetic inductance has been exploited previously to make wideband traveling-wave amplifiers in coplanar waveguide (CPW) transmission lines of NbTiN [19]. In these devices, dispersion is geometrically engineered because there is no intrinsic frequency dispersion (within 5% measurement accuracy) up to $f_{\max} \cong 2\Delta/h \times 66\%$ [20]. For NbTiN, this corresponds to frequencies on the order of 600 GHz.

Half wave CPW resonators fabricated from 20 nm thick NbTiN films were used, and comb generation was observed up to $T \sim 6$ K due to the high $T_C \sim 13$ K of the films. The geometries used included both transmission, illustrated in Fig. 1, and reflection, described in [21]. The unperturbed fundamental resonant frequency for these resonators is given by $f_0 = \omega_0/2\pi = c\sqrt{1-\alpha}/(2ln_{\text{eff}})$, where l is the length, $n_{\text{eff}} = 2.6$ is the effective index of refraction for a CPW on Si, and $\alpha = 0.93$ is the kinetic inductance fraction as determined from the frequency shift of a test resonator. We were thus able to set f_0 in the range of 15 MHz up to 6 GHz with easily achievable lengths from 1 m down to 2.5 cm. For clarity and brevity, the discussion here is restricted to a single device, a 25 cm long NbTiN resonator with $f_0 = 59.738181(1)$ MHz. The design, fabrication, and theoretical analysis are described in the Supplemental Material [22].

Frequency comb emission is excited in these devices by applying a pump tone at frequency f_P. With $f_P = Nf_0 + \delta f$, power is coupled into the resonator at both f_P and f_0 when the detuning, δf, is decreased. The value of N is selected by adjusting the pump power prior to fine-tuning δf. Moreover, in addition to output at the fundamental and pump frequencies, the nonlinear resonance is characterized by a new set of subharmonic states, distinct from natural modes of the resonator cavity, that form at odd harmonics of both the resonance and pump frequencies. Unlike the case of linear response, proximity of f_P to f_0 is

FIG. 1 (color). Photograph of superconducting frequency comb chip. The 25 cm long, $\lambda/2$ resonator is made in a coplanar waveguide (CPW) geometry with input (output) port at top left (bottom right). The CPW has a 2 μm wide center strip and 2 μm wide gap and is coupled to ports by interdigitated capacitors. The device is made from NbTiN (Au color) on a 2 cm $\times$ 2 cm intrinsic Si (> 20 kΩ) substrate.

not a requirement. Quite the contrary, f_P can be spectrally distant from f_0, i.e., $N \gg 1$, with strong nonlinear response elicited as δf is decreased.

In particular, for constant pump power, as δf, and hence f_P, is decreased, the current induced in the resonator renormalizes f_0 downward due to the dependence of the kinetic inductance on current [23]. As δf approaches zero, state bifurcation invariably occurs and the resonator jumps back to a quiescent state at some critical frequency $f_P = f_{\text{crit}}$ [24]. However, prior to this event, enough power may be coupled into the resonator to cross the parametric oscillation threshold wherein the gain exceeds cavity losses. This condition permits steady-state generation of a full range of frequency sidebands and FWM products [24], seeded by pump-harmonic states.

To explain our results, we introduce a simple LC transmission-line model, as in (a) of Fig. 2. The model neglects higher normal modes of the resonator cavity because our investigations with two-tone spectroscopy have shown that higher normal modes are inert. Instead, observed resonances are of extremely narrow linewidth, indicative of states that do not couple readily to a dissipative reservoir. When the circuit of the figure is analyzed, the output current $I_o(t)$ satisfies

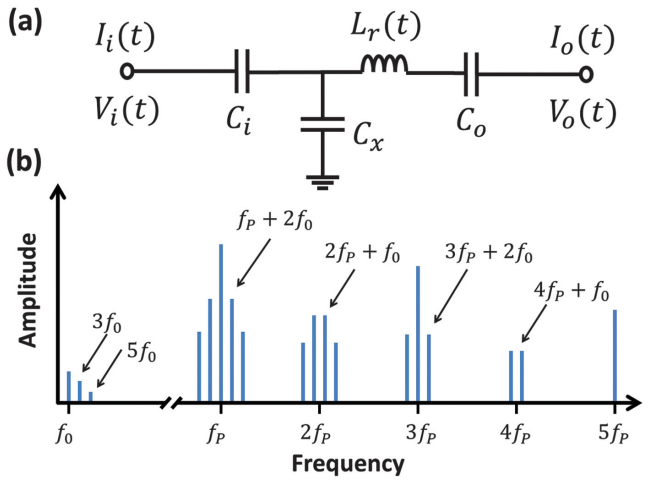

FIG. 2 (color). Panel (a) depicts model circuit while (b) shows sideband spectrum predicted by second-order perturbation theory. Illustrated are fundamental f_0 and pump f_P frequencies, as well as initially generated sideband frequencies, spaced $2f_0$ apart, as dictated by the selection rule.

$$\frac{d^2A(t)}{dt^2} + \omega_0^{(0)2}A(t) + \frac{1}{3}\frac{d^2A(t)^3}{dt^2} = F\cos\omega_P t, \qquad (1)$$

with $A(t) = I_o(t)/I_*$, undressed fundamental $\omega_0^{(0)} = \sqrt{(C_i + C_o + C_x)/L_o(C_i + C_x)C_o}$, pump frequency $\omega_P = 2\pi f_P$, and effective driving term $F = \omega_P \bar{V}/I_* L_o$. Here, $\bar{V}$ is the amplitude of an effective voltage drop across the line. Details of the model derivation may be found in the Supplemental Material [22]. Equation (1) is similar to that of a Duffing oscillator [25], which is known to exhibit subharmonic generation [26].

Successive approximation perturbation theory [27] is applied to Eq. (1) to demonstrate important characteristics of the observed nonlinear response, including (i) the existence of nonlinear states, (ii) the frequency spacing between them, (iii) the selection rule of their allowed occupation, and (iv) the renormalization of the fundamental frequency. The procedure is to expand both the dressed fundamental frequency $\omega_0 = 2\pi f_0$ and the amplitude $A(t)$ in powers of mathematical device ϵ, apply the expansions to Eq. (1), equate terms of same power of ϵ, remove secular terms at each order that would otherwise lead to divergence, and set $\epsilon = 1$ at the end of calculation. Secular terms are associated with the fundamental frequency; setting these to zero at each successive order in ϵ defines the renormalization corrections of ω_0.

Specifically, we write $\omega_0 = \omega_0^{(0)} + \epsilon\omega_0^{(1)} + \epsilon^2\omega_0^{(2)} + \cdots$ and $A(t) = A_0^{(0)}(t) + \epsilon A_0^{(1)}(t) + \epsilon^2 A_0^{(2)}(t) + \cdots$, and assuming a strong pump such that the zero-order amplitude is of the form

$$A_0^{(0)}(t) = C_o\cos\omega_0 t + \frac{F}{\omega_P^2 - \omega_0^2}\cos\omega_P t, \qquad (2)$$

the expansion is applied to Eq. (1). Results are summarized here to second order in ϵ using initial conditions $A(0) = 0$ and $\dot{A}(0) = 0$, with details of the algebra provided in the online supplement. Our calculation shows the second-order $A(t)$ sketched in (b) of Fig. 2, with fundamental frequency approximated as

$$\omega_0 \cong \omega_0^{(0)}\left(1 - \frac{3}{8}\frac{F^2}{\omega_P^4} + \frac{745}{768}\frac{F^4}{\omega_P^8}\right); \qquad F \ll \omega_P^2. \tag{3}$$

Panel (b) of Fig. 2 depicts how nonlinear states form within sidebands as a consequence of beating between the two frequencies f_0 and f_P, and how these states are separated in frequency by $2f_0$, in accordance with a selection rule that arises from the from of the kinetic inductance, and ultimately, the symmetry of the film geometry. In particular, Eq. (3) indicates that the fundamental frequency is downshifted, as is, therefore, the spacing between states, which we have observed experimentally. Sideband states, at least in the precascade regime, may be summarized as follows:

(i) odd harmonics of the pump, Mf_P, where $M = 1, 3, 5, \ldots$, are permitted as principal teeth of the comb,

(ii) sideband teeth spaced at $2f_0$ are generated around the odd pump harmonics,

(iii) even harmonics of the pump, with $M = 0, 2, 4, \ldots$ are forbidden, and

(iv) sideband teeth spaced at $2f_0$ are generated around the absent even pump harmonics.

For integer $M \geq 0$, the allowed frequencies of these rules are

$$\begin{aligned} &f_0, 3f_0, 5f_0, \ldots; M = 0, \\ &Mf_P, Mf_P \pm 2f_0, Mf_P \pm 4f_0, \ldots; M \text{ odd}, \\ &Mf_P \pm f_0, Mf_P \pm 3f_0, \ldots; M \text{ even}. \end{aligned} \tag{4}$$

Measurements of the frequency emission spectrum were conducted at low temperature, $T = 3$ K, in a magnetically unshielded copper box. An rf signal generator was connected to the input to excite the system and a spectrum analyzer was connected to the output. The experiments described here used pump powers of $-28(1)$ dBm with detuning $\delta f \sim 100$ kHz.

Figure 3 shows a typical evolution of the spectrum as f_p is decreased to the point of bifurcation. For convenience, we define $\Delta f = f_P - f_{\text{crit}}$. Far from bifurcation, above $\Delta F = 1200$ kHz, we see predominantly odd multiples of the pump in the spectrum, i.e., just the principal teeth of odd sidebands. Some emission at $2f_P$ and $4f_p$ is observed, albeit at -25 dB relative to the odd harmonics and can be accounted for by distortion in the amplifier and/or parasitic slot-line modes. The amplifiers also had a low frequency

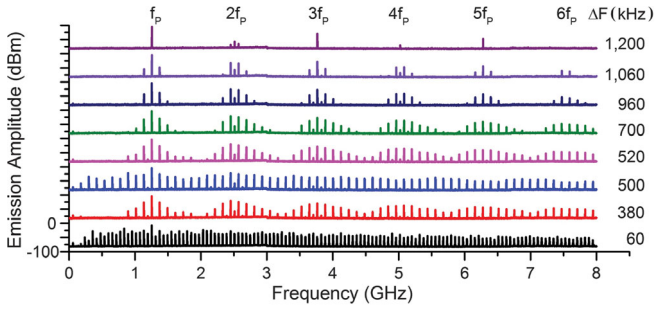

FIG. 3 (color). Evolution of emission spectrum as difference, $\Delta F = f_P - f_{\text{crit}}$, between pump frequency f_P and critical bifurcation frequency, $f_{\text{crit}} = 1254.7$ MHz, is decreased. The pump is close to the $N = 21$ multiple of the resonator fundamental, f_0. Sample is held at $T = 3$ K, with pump power of feedline held constant at -28 dBm. Traces are offset vertically for clarity. Signal has been amplified by 30 dB. (Finer detail as $\Delta F \to 0$ may be found in successive frames of the video of the Supplemental Material [22], where each frame is equivalent to a trace of above stack plot.)

cutoff below 500 MHz, thereby filtering out the response at $f_0 \cong 60$ MHz.

As ΔF approaches 1200 kHz, sideband teeth spaced by $2f_0$ are first observed around the $2f_P$ location, shown in the top spectrum of Fig. 3. At $\Delta F = 1{,}060$ kHz, sideband teeth begin to appear around both even and odd multiples of the pump, as described by Eq. (4). The full width at half maximum (FWHM) of the sideband peaks is the same across the spectrum and measured to be 1.1(0.1) Hz, limited most likely by the resolution bandwidth of the spectrum analyzer. This is nearly an order of magnitude less than that expected from a $Q = 10^7$ resonator, consistent with states that do not couple to a dissipative reservoir. These sidebands continue to develop down to $\Delta F = 520$ kHz. As ΔF continues to decrease and the system is pushed closer to bifurcation, the sideband structure undergoes a sudden transition, coalescing into a continuous, broadband comb structure at $\Delta F = 500$ kHz. This structure can persist to well above 20 GHz, depending on the specific f_P and power used. The upper limit of the response readout is currently limited by the connectors (SMA) used on the system, but even with this configuration, we see cascades spanning at least six octaves in frequency.

The system undergoes two more transitions as it nears perfect tuning. The second transition, at $\Delta F = 380$ kHz, occurs where it switches back into a modulated broadband comb, and the final, third transition, at $\Delta F = 60$ kHz, sees it coalesce again into a smooth spectrum with a modified spacing between sidebands of $1 \times f_0$. The comb then collapses as $\Delta F \to 0$, and the system goes past a bifurcation point.

The change in the sideband spacing is consistent with period doubling that typically occurs in nonlinear systems

as they go through bifurcations [28]. This interpretation is supported by data taken for varying values of pump power, where period doubling is always observed just before bifurcation, even at low power. This observation rules out other effects such as amplifier saturation or power-dependent modes in the CPW. This evolution of behavior is repeated, albeit in a slightly modified nature, for pumps with different subharmonic matching. We also note that for phases with continuous, coalesced sidebands (around $\Delta F = 500$ and 60 kHz), multiple satellite peaks appear around the comb teeth with frequency spacing $\sim\delta f$. This indicates that separate sidebands from the various multiples of the pump are beating together, owing to the many-octave extent of the entire broadband structure.

In order to accurately measure the spacing of the sidebands, a nonlinear mixing process is employed. In this measurement, the output signal is split into two components. One component is amplified and applied to the local oscillator (LO) input of a wideband mixer. The other component is then applied to the rf input, where each tooth of the comb is compared to the inputs. Each comb tooth therefore acts as a reference for all other teeth, giving an output that reflects the overall comb periodicity. Using this technique, the FWHM of the periodicity was measured to be less than 1 Hz, corresponding to frequency resolution better than one part in 10^8. Drift in the periodicity on the order of 10 Hz occurs on the 10 to 100 second time scale, with characteristic jumps consistent with flux trapping in the CPW gap.

Another exciting aspect of these devices is that it is possible to measure the signal in both the time and the frequency domain for devices with reasonably low f_0. To accomplish this, the same device was pumped with a much higher frequency. A low pass filter was then used to separate the signal from the pump. A graph of the resulting time domain response from a pumping near $147 \times f_0$ is shown in Fig. 4. Full movies of both the time and spectral response are available either from the authors or in the Supplemental Material [22]. While the response from pumping close to different harmonics gives different results, qualitatively, we observe behavior similar to that described above. At this particular harmonic, we first see a $3 \times f_0$ component as the comb lights, at about 12.6 MHz from the bifurcation point. The $1 \times f_0$ and $2 \times f_0$ behaviors appear to compete as the detuning is decreased, and the system begins pulsing strongly just before the comb collapses. An important aspect of these curves is that they conclusively show that the comb frequencies are phase locked. This is most clear around 7.4 MHz detuning, where the evidence of both the first harmonic and multiple higher harmonics are superimposed on the $2 \times f_0$ oscillation.

In conclusion, we have demonstrated and theoretically modeled broadband frequency-comb generation in highly nonlinear superconducting resonant cavities. We have fabricated and tested multiple devices with different materials and free-spectral ranges and find highly reproducible and reliable behavior. The stability of the comb generation is expected to improve as magnetic shielding and multiple-octave feedback is added [9]. The low loss and lack of dispersion allow for multiple decades of comb generation. Since the temperatures needed are achievable with a closed cycle He compressor, we expect that these devices will allow for relatively low-cost, frequency-agile devices in the near future. The simplicity of these devices, their low dispersion, high nonlinearity, and the fact that they can be easily measured with standard rf techniques make them an exciting platform to study nonlinear phenomena.

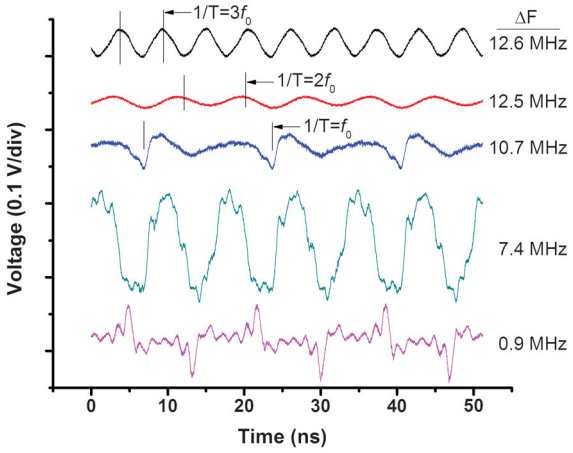

FIG. 4 (color). Time domain response of 60 MHz nonlinear resonator driven above the 147th harmonic, at 8820 MHz. Movies depicting the evolution of the above time series, as well as the corresponding frequency response, with decreasing detuning, are included as video in the Supplemental Material [22].

For important insights, the authors are grateful for helpful discussions with Jiansong Gao, Pascal Del'Haye, Scott Diddams, Dave Howe, Dylan Williams, and Dan Slichter. We also acknowledge Aric Sanders and the Precision Imaging facility at NIST. This work was supported by DARPA and the NIST Quantum Information initiative. R. P. E. acknowledges Grant No. 60NANB14D024 from the U.S. Department of Commerce, NIST. This work is property of the US Government and not subject to copyright.

*David.Pappas@NIST.gov

[1] I. Coddington, W. C. Swann, and N. R. Newbury, Phys. Rev. A **82**, 043817 (2010).
[2] D. Yu, C. Park, W. Lee, S. Lee, S. Park, J. Mun, S. Lee, and T. Kwon, J. Korean Phys. Soc. **63**, 883 (2013).
[3] A. Hati, C. Nelson, C. Barnes, D. Lirette, T. Fortier, F. Quinlan, J. DeSalvo, A. Ludlow, S. Diddams, and D. Howe, IEEE Trans. Ultrason. Ferroelectr. Freq. Control **60**, 1796 (2013).
[4] P. Del'Haye, A. Schliesser, O. Arcizet, T. Wilken, R. Holzwarth, and T. J. Kippenberg, Nature (London) **450**, 1214 (2007).

[5] P. Del'Haye, T. Herr, E. Gavartin, M. L. Gorodetsky, R. Holzwarth, and T. J. Kippenberg, Phys. Rev. Lett. **107**, 063901 (2011).
[6] M. A. Foster, J. S. Levy, O. Kuzucu, K. Saha, M. Lipson, and A. L. Gaeta, Opt. Express **19**, 14233 (2011).
[7] S. Fang, H. Chen, T. Wang, Y. Jiang, Z. Bi, and L. Ma, Appl. Phys. Lett. **102**, 231118 (2013).
[8] S. B. Papp, P. Del'Haye, and S. A. Diddams, Phys. Rev. X **3**, 031003 (2013).
[9] P. Del'Haye, O. Arcizet, A. Schliesser, R. Holzwarth, and T. J. Kippenberg, Phys. Rev. Lett. **101**, 053903 (2008).
[10] T. J. A. Kippenberg, Ph.D. thesis, California Institute of Technology, 2004.
[11] I. H. Agha, Y. Okawachi, and A. L. Gaeta, Opt. Express **17**, 16209 (2009).
[12] Y. K. Chembo and N. Yu, Phys. Rev. A **82**, 033801 (2010).
[13] Y. K. Chembo, D. V. Strekalov, and N. Yu, Phys. Rev. Lett. **104**, 103902 (2010).
[14] T. Hansson, D. Modotto, and S. Wabnitz, Phys. Rev. A **88**, 023819 (2013).
[15] C. Godey, I. V. Balakireva, A. Coillet, and Y. K. Chembo, Phys. Rev. A **89**, 063814 (2014).
[16] P. K. Day, H. G. Leduc, B. A. Mazin, A. Vayonakis, and J. Zmuidzinas, Nature (London) **425**, 817 (2003); B. A. Mazin, B. Bumble, P. Day, M. E. Eckart, S. Golwala, J. Zmuidzinas, and F. A. Harris, Appl. Phys. Lett. **89**, 222507 (2006).
[17] R. Barends, N. Vercruyssen, A. Endo, P. J. de Visser, T. Zijlstra, T. M. Klapwijk, P. Diener, S. J. C. Yates, and J. J. A. Baselmans, Appl. Phys. Lett. **97**, 023508 (2010).
[18] *Handbook of Superconducting Materials*, edited by D. A. Cardwell and D. S. Ginly (IOP Publishing, London, 2003), Vol. 1.
[19] B. H. Eom, P. K. Day, H. G. LeDuc, and J. Zmuidzinas, Nat. Phys. **8**, 623 (2012).
[20] H. H. S. Javadi, W. R. McGrath, B. Bumble, and H. G. LeDuc, in *Proceedings of the Third International Symposium on Space Terahertz Technology* (University of Michigan, Ann Arbor, 1992), p. 362.
[21] D. S. Wisbey, J. Gao, M. R. Vissers, F. C. S. da Silva, J. S. Kline, L. Vale, and D. P. Pappas, J. Appl. Phys. **108**, 093918 (2010).
[22] See Supplemental Material at http://link.aps.org/supplemental/10.1103/PhysRevLett.113.187002 for design, fabrication, theory derivations, and additional video material.
[23] A. Karpov, D. Miller, F. R. Rice, J. A. Stern, B. Bumble, H. G. LeDuc, and J. Zmuidzinas, Proc. SPIE Int. Soc. Opt. Eng. **5498**, 616 (2004).
[24] L. J. Swenson, P. K. Day, B. H. Eom, H. G. Leduc, N. Llombart, C. M. McKenney, O. Noroozian, and J. Zmuidzinas, J. Appl. Phys. **113**, 104501 (2013).
[25] G. Duffing, *Erzwungene Schwingungen bei Veranderlicher Eigenfrequenz* (F. Vieweg u. Sohn, Braunschweig, 1918).
[26] M. E. Levinson, J. Appl. Phys. **20**, 1045 (1949); C. Holmes and P. Holmes, J. Sound Vib. **78**, 161 (1981); D. W. Jordan and P. Smith, *Nonlinear Ordinary Differential Equations: An Introduction for Scientists and Engineers*, 4th ed. (Oxford University Press, Oxford, 2007), p. 242.
[27] L. D. Landau and E. M. Lifshitz, *Mechanics*, 3rd ed. (Pergamon Press, Oxford, 1976), p. 84.
[28] D. W. Jordan and P. Smith, *Nonlinear Ordinary Differential Equations: An Introduction for Scientists and Engineers*, 4th ed. (Oxford University Press, Oxford, 2007), p. 447; S. H. Strogatz, *Nonlinear Dynamics and Chaos* (Perseus Books Publishing, Cambridge, 2000), p. 379.